nature physics

Article

https://doi.org/10.1038/s41567-022-01857-9

Nonlinear multi-frequency phonon lasers with active levitated optomechanics

In the format provided by the authors and unedited

Content

1. EXPERIMENTAL SYSTEM

1.1 PHONON LASINGS IN VARIOUS OPTOMECHANICAL SYSTEMS

Table 1 shows the phonon lasing behaviours in various optomechanical systems. We note that the size or the mass of our micro-sphere is 3 to 4 orders larger than the nano-sphere. Moreover, our system is governed by the dissipative LOM coupling, due to much stronger optical scattering losses by much larger objects, in contrast to the dispersive LOM coupling in previous works dealing with nanoscale objects. In addition, not only a fundamental-mode phonon laser, but also nonlinear mechanical harmonics are observed, including their lasing threshold feature and higher-order mechanical correlations.

Table S1| Optomechanical systems for phonon lasing

Features	WGM cavity[S1]	F-P cavity[S2]	Passive LOM system[S3]	Active LOM system
Optical gain	✗	✗	✗	✓
Optomechanical coupling	Dispersive	Dispersive	Dispersive	Dissipative
External feedback	✗	✗	✓	✗
Size of the oscillator	~ 50 μm	~ 1 mm	~ 0.1 μm	~ 2 μm
Mass of the oscillator	~ 10^{-9} kg	~ 10^{-9} kg	~ 10^{-18} kg	~ 10^{-14} kg
Mechanical frequency	10 ~ 100 MHz	~ 100 kHz	~ 100 kHz	~ 10 kHz
Harmonics	✗	✗	✗	✓

Notation: WGM, whispering-gallery-mode; F-P, Fabry-Pérot; ✓ for Yes; ✗ for No.

Particularly, the nonlinearity in our work is different from the nonlinear feedback in the passive LOM system [S3]. Firstly, the fundamental origins of non-linearities are different. In Ref. [S3], the coupling between the laser and the oscillator is artificial since a series of external devices are used for feedback control, e.g., an acousto-optic modulator, a digital lock-in amplifier, a phase shifter, etc. These external devices can help to monitor the feedback parameters and achieve feedback control. In contrast, in our dissipative LOM system, the coupling of the oscillator and the cavity emerges autonomously, without any need of all the above-mentioned feedback/monitor devices.

We note that the dissipative coupling in our system reaches 10^{12} Hz/m, comparable to the dispersive coupling in previous LOM works. That means a small shift in oscillator's position can lead to strong change in the cavity power and thus strong

nonlinear optical force experienced by the oscillator.

Secondly, the nature of our phonon laser is clearly different from the previous one: Ref. [S3] have presented experimental evidence for phonon lasing for the fundamental mode, while in our experiment, we observe for the first time the harmonics of the fundamental mechanical mode, including their lasing thresholds and second- or higher-order correlations.

Finally, we note that Ref. [S3] applied a modulation signal $\propto q_i\dot{q}_i$ to achieve non-linear cooling, as a standard parameter feedback method to bring in optical damping and to counteract the oscillator's motion [S4]. This method can regulate the total damping of the system but is independent of the total force distribution, while in our system, due to the dissipative coupling, the optical power of the cavity field can change when the oscillator moves and thus leads to nonlinear optical force on the oscillator.

1.2 OPTOMECHANICAL COUPLING STRENGTH

We use an order of magnitude larger sphere than that in Ref. [S3] in our active LOM system, which is central to enhancing the dissipative coupling and thus observing nonlinear multi-frequency phonon lasing. In fact, compared with Ref. [S3], the cavity mode volume of our system is 5 orders larger, with a much larger free-space optical path; thus in our system, even by using a nano-sphere, the dissipative coupling (5.0×10^9Hz/m) is still 2 orders higher than the dispersive part (1.4×10^7 Hz/m), and more importantly, no phonon lasing can be observed at all in this case. For our micro-sphere phonon-laser, the dissipative coupling of (1.4×10^{12}Hz/m) is significantly enhanced for ~300 times in comparison with that of the nano-sphere, which is central to observing the nonlinear phonon laser in our experiment.

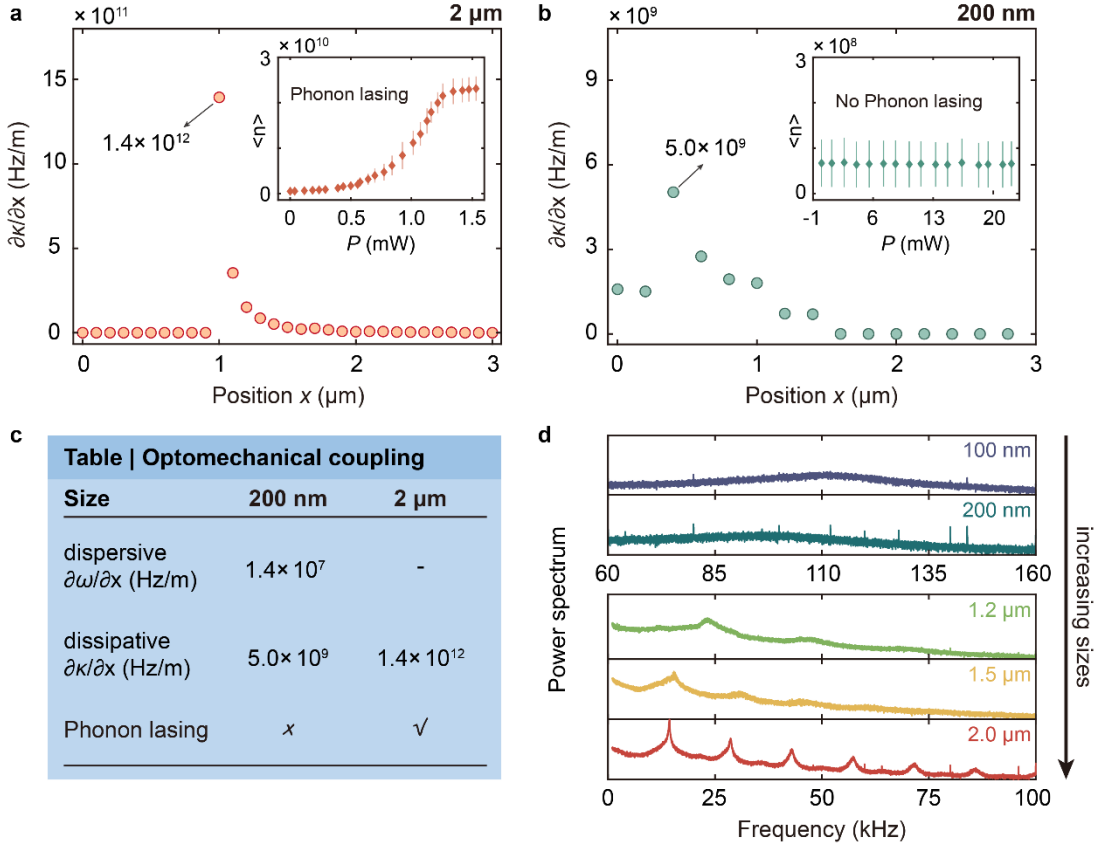

Table | Optomechanical coupling

Size	200 nm	2 μm
dispersive $\partial\omega/\partial x$ (Hz/m)	1.4×10^{7}	-
dissipative $\partial\kappa/\partial x$ (Hz/m)	5.0×10^{9}	1.4×10^{12}
Phonon lasing	×	√

Figure S1.2. Dissipative coupling strength. a, Dissipative coupling strengths of 2 μm and **b,** 200 nm spheres versus spheres' offset distance. Insets show the mean phonon number <*N*> versus intracavity power P (mW). The dots are mean values. Error bars denote ±1 s.d. of each measurement, consisting of 5×10^5 samples. **c,** A comparison of dispersive and dissipative optomechanical couplings for nano- and micro-spheres. Here, the dispersive optomechanical coupling of the micro-sphere (-) cannot be calculated by the Rayleigh scattering theory. **d,** The power spectra of different sizes spheres.

Specifically, for a trapped nano-sphere, due to the Rayleigh scattering, a dispersive change in the optical path length can shift the cavity resonance frequency, which can be quantified as [S5]:

$$U_0(x_0)=\frac{\omega_{cav}\xi}{2\varepsilon_0 V_{cav}}\left(1+\frac{x_0^2}{x_R^2}\right), \tag{S1.1}$$

where ω_{cav} is the cavity frequency, V_{cav} is the mode volume; x_R is the Rayleigh length, x_0 is the distance between the sphere's position and the cavity center, and ε_0 is vacuum permittivity. For a nanosphere with radius r, the polarizability can be written as [S6]:

$$\xi=4\pi r_0^3\varepsilon_0\,\mathrm{Re}\left(\frac{\varepsilon-1}{\varepsilon+2}\right). \tag{S1.2}$$

For our experimental parameters: r_0 = 100 nm, ε = 2.1, $\varepsilon_0 = 8.86\times10^{-12}$ *F*/m, $\omega_{cav} = 6\pi\times10^{14}$ rad/s, $V_{cav} = 1.4\times10^{-6}$ m^3, $x_0 = 0$, we can estimate the maximum frequency shift

as 2.26Hz, which is negligible compared to the laser frequency ~ 10^{14} Hz or the laser linewidth ~ 10^{6} Hz. For the longitudinal direction of the cavity mode, the dispersive coupling strength is:

$$\partial\omega / \partial x = U_0\left(x_0\right)\sin(2k \cdot dx)k\,, \tag{S1.3}$$

where $k = 2\pi/\lambda$, dx is the longitudinal position of the nano-sphere with respect to the intensity maximum x_0. By setting $\sin(2k \cdot dx) = 1$, the maximum dispersive coupling is estimated as 1.4×10^{7} Hz/m. For the vertical direction of the cavity mode, the dispersive coupling strength is:

$$\partial\omega / \partial r = U_0\left(x_0\right)\partial I / \partial r = U_0\left(x_0\right)\frac{-2r}{\omega_0{}^2} I_0 e^{-\frac{r^2}{\omega_0{}^2}}\,, \tag{S1.4}$$

where r is the vertical position, ω_0 is the beam waist of the Gaussian beam, and I or I_0 denotes the vertical intensity distribution of the Gaussian beam or the normalization coefficient. The maximum dispersive coupling is estimated as 1.5×10^{6} Hz/m. Clearly, both longitudinal and vertical dispersive couplings are 5 orders lower than nano-sphere LOM system ~ 10^{12} Hz/m [S5]. For a micro-size sphere, we have tried to detect the frequency shift by loading the sphere to the cavity, but we find that it is too small to be detected.

The dissipative coupling strength of the system can also be estimated by calculating cavity loss scattered by the sphere [S7]. Above the threshold, the laser power is described by:

$$P(\rho) = P_0\left[\frac{\mu P_{pump}}{\delta_i + \delta_s\left(\rho\right)} - 1\right], \tag{S1.5}$$

where P_0 is the saturation power, μP_{pump} is the round-trip gain, δ_{i} is the cavity loss independent of the sphere's position, determined by the pumping power P_{pump} and the gain medium, δ_{s} is the scattering loss determined by the sphere's position ρ. Once we obtain the relation curve between P and δ_{s}, the scattering loss δ_{s} per displacement of the trapped sphere can be expressed as:

$$\frac{\partial\delta_s}{\partial x} = \frac{\mu P_{pump} P_0}{\left(P + P_0\right)^2} \cdot \frac{\partial P}{\partial x}\,, \tag{S1.6}$$

Then, the dissipative coupling strength can be written as:

$$\frac{\partial \kappa}{\partial x} = \frac{c}{2\pi L} \cdot \frac{\partial \delta_s}{\partial x}, \tag{S1.7}$$

The beam waist of our system ~1.3 μm is much smaller than that in the previous LOM system ~ 41μm [S5], resulting in enhanced scattering and thus dissipative coupling. Fig. R2.1 shows the dissipative coupling for different-size spheres. The insets illustrate the intracavity optical power as a function of the sphere's position. We find that the dissipative coupling of the micro-sphere (1.4×10^{12}Hz/m) is ~300 times higher than that of the nano-sphere (5×10^{9}Hz/m), which is also 2 orders of magnitude higher than dispersive coupling. We have confirmed that no phonon lasing can be achieved by using nano-spheres (e.g., 100 nm or 200 nm sphere) in our present setup.

1.3 RESPONSE OF THE ACTIVE CAVITY

A major advantage of an active cavity is the narrower linewidth compared to the passive one and thus supports a longer photon lifetime. This in turn contributes as a mechanical gain to the sphere oscillator. To directly emphasize this advantage, we study the time evolution of the sphere's position and the optical power, when the oscillator experiences coherent dynamics. Results depicted in Fig. S1.3a imply that the phase of the laser power lags behind the oscillator's motion with a retardation time of around 5 ~ 10 μs.

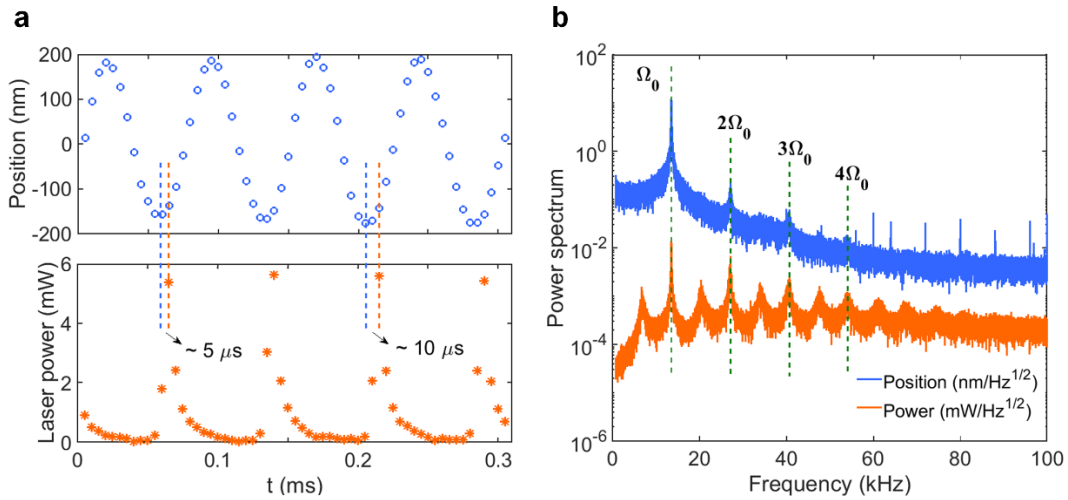

Figure S1.3. Response of the active cavity. a, Time evolution of sphere's position and intracavity optical power. **b,** Comparison of the power spectrum of sphere position and intracavity laser power when phonon lasing emerges. The peaks at frequencies greater than 50 kHz are noise from the trapping laser (wavelength, 532 nm).

Figure S1.3b shows power spectra of the sphere's position and intracavity laser when the oscillator experiences a coherent dynamic. The phonon lasing with high order harmonics occurs due to the strong dissipative optomechanical coupling. In addition, we find that the spectrum of the laser power shows lots of peaks, including half frequency $0.5\Omega_0$ and its multiple components. We attribute that to the nonlinear response of the intracavity optical power to the sphere's position.

1.4 POWER SPECTRUM OF OSCILLATOR'S POSITION

The optical power of dual-beam optical tweezer (wavelength, 532 nm) controls the oscillation frequency of the sphere-oscillator. Thus, we can modulate the phonon laser's frequency by tuning the trapping power. Figure S1.4 illustrates this capability for three specific trapping powers.

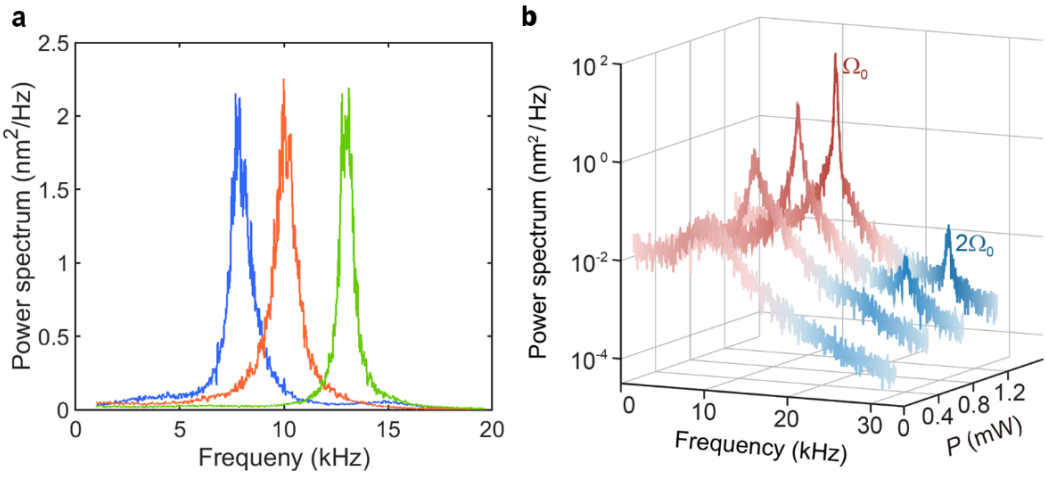

Figure S1.4. Power spectra of the oscillator's motion. a, Tuning of the phonon laser's frequency by the power of the trapping laser (wavelength 532 nm):300 mW (blue), 325 mW (red) and 350 mW (green). **b,** Phonon power spectra versus oscillation frequency for different intracavity powers of the active cavity (centered at 1030 nm). Phonon laser with double frequency is clearly observed at powers greater than 0.78 mW.

Intriguingly, we observe a nonlinear phonon laser with double frequency $2\Omega_0$. Figure S1.4b shows the power spectra of the oscillator for different intracavity mean powers. By increasing the power, a frequency-doubled component emerges. The intensity of this higher-order harmonics is weaker than that of the fundamental frequency Ω_0. We study the mean phonon population at $2\Omega_0$ by filtering the thermal phonons and the phonons with Ω_0. It is worth to point out that these nonlinear phonon

lasing behaviours featuring multiple frequencies are different from the single-mode phonon lasers or the multi-mode phonon lasers, in which only a single oscillating mode can be stimulated into the lasing regime because of the mode competition.

1.5 HARMONICS OF THE FUNDAMENTAL MECHANICAL MODE

The harmonics of the fundamental mechanical mode can be observed from the time domain, as shown in Fig S1.5a. It illustrates the spatial distribution of the microsphere for various resonances Ω_0, $2\Omega_0$, $3\Omega_0$ with the numbers of nodes 10, 20, 30, respectively. The number of nodes and anti-nodes is commensurate with the various harmonics.

In addition, to eliminate the doubled or tripled effect arising from the measurement electronics, we implement a higher-power laser on the HBD detection system (10 times higher than that taken in our main text) and a 10 kHz modulation signal is added to the laser through a modulator, as shown in Fig. S1.5b. Clearly, no doubled or tripled component emerges even for this case.

Our work here is essentially different from parametric amplification [S8]. First, the mechanical parametric amplification originates from the nonparabolicity of the optical potential, which typically dominates in the μm region for motional displacement (see also Fig. 2.6 in Ref. [S9]). In contrast, in our work, the maximum displacement of the oscillator is ~300 nm, which is small enough and thus far away from the region of observing mechanical parametric amplification. In fact, in our work, the nonlinear optical force comes from the dissipative coupling of the cavity field and the micro-sphere, which exists even for a smaller displacement (see Fig. S1.3a).

Secondly, in the mechanical parametric amplification system, the nonparabolicity of optical potential can lead to not only frequency multiplying, but also frequency shifting. When the oscillator experiences larger displacement, the absolute value of the optical force is a convex function, the slope of which (and thus the natural frequency of the oscillator) decreases (see Fig. 3c in Ref. [S8]). In contrast, in our work, the natural frequency increases above the lasing threshold (see Fig. 1b in the main text).

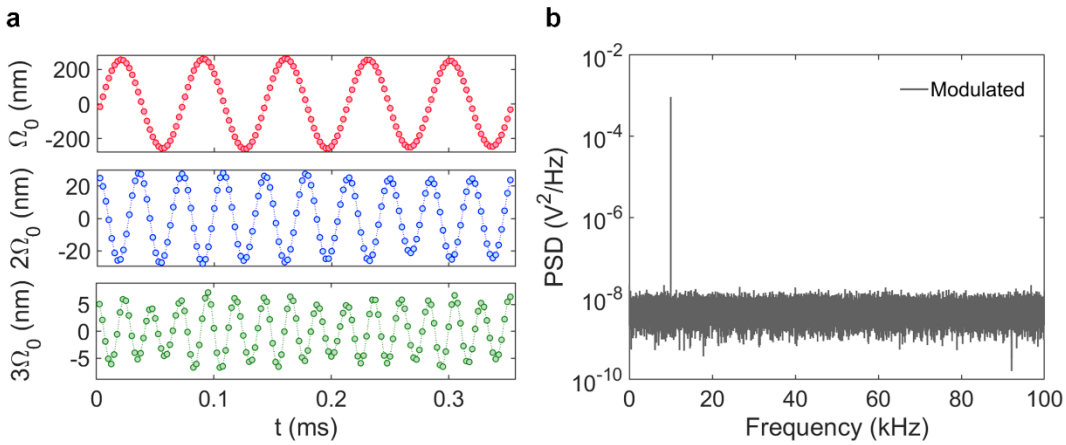

Figure S1.5. Harmonics of the fundamental mechanical mode. a, Time evolution of spatial distribution of the fundamental mechanical mode Ω_0, and its harmonics $2\Omega_0$, $3\Omega_0$. **b,** Power spectrum of the HBD output when a 10 kHz modulated signal acts on the sensor.

2. NONLINEAR OPTICAL FORCE

2.1. OPTICAL FORCE AND OPTICAL DAMPING RATE

The temporal evolution of a sphere's position $x(t)$ can be described by a harmonic oscillator,

$$m\ddot{x} + m\Gamma_g \dot{x} + m\Omega_0^2 x = F_{opt}(x) + F_{th}, \tag{S2.1}$$

where m represents the mass of the oscillator, Ω_0 is the natural frequency. The gas damping Γ_g for a sphere with a radius R is given by [S10]

$$\Gamma_g = \frac{6\pi\eta R}{m}\frac{0.619}{0.619+Kn}\left(1+\frac{0.31}{0.785+1.152Kn+Kn^2}\right), \tag{S2.2}$$

where η is dynamic viscosity of air, $Kn = l/R$ is the Knudsen number, and l is mean free path of gas. F_{th} is the Brownian force, $F_{opt}(x) = Q(x)P$ is the optical force from the active cavity along x-axis, where $Q(x)$ and P are trapping efficiency and trapping power, respectively.

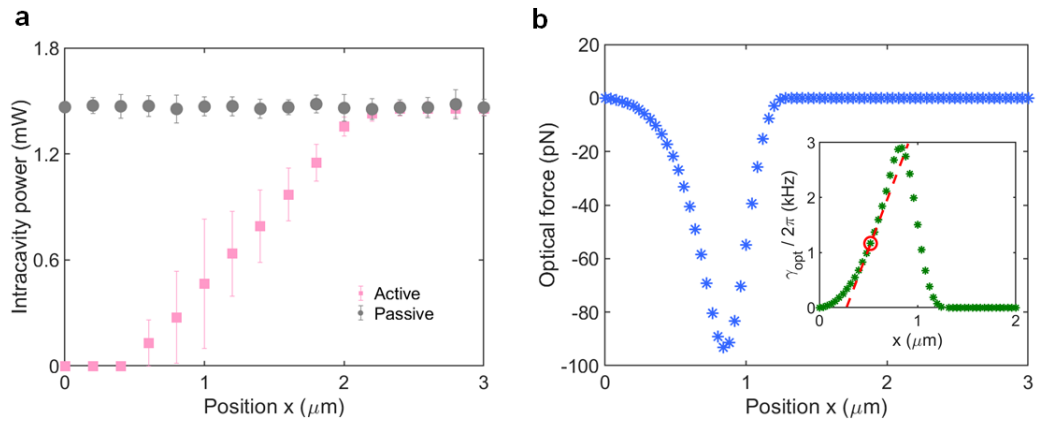

Figure S2.1. Intracavity laser power and optical force. a, Experimental result for intracavity laser power as a function of the sphere's position in the active and passive setups. Data are presented as mean values and error bars denote ±1 s.d. of each measurement, consisting of 10 samples. **b,** Simulation result of optical force and optical damping rate γ_{opt} (inset map) in the active cavity. The red-dashed line is the fitted result for a selected working point.

Figure S2.1a shows the intracavity laser power in the active and passive systems, when we adjust the sphere's position. For the case of the passive system, the photon lifetime is relatively short and thus the optomechanical coupling between the cavity field and the sphere is weak. Result shows that the intracavity laser power P is independent of the sphere's position x. Thus, the optical force in the passive setup can be written as, $F_{passive}(x) = Q(x)P$. However, the photon lifetime in the active setup is longer. The sphere in the active setup alters the cavity loss, i.e., dissipative coupling, and hence the intracavity laser power P is modulated by the sphere's position (see Figure S2.1a). As a result, the optical force in the active setup can be written as $F_{active}(x) = Q(x)P(x)$.

Considering the delay response of the cavity, the trapping power $P(x,t)$ is a function of time t. It can be written as $P(x,t) = P(x(t-\tau))$, where τ is the retardation when a change in x emerges. Applying the Taylor expansion, $P(x,t)$ can be written as $P(x,t) = P(x(t) - \tau\dot{x}(t)) = P(x) - \tau\dot{x}(t)dP/dx$. Then, the optical force $F_{opt}(x,t)$ in the Eq. (S2.1) can be written as,

$$F_{opt}(x,t) = \underbrace{Q(x)P(x)}_{Optical\ \ force} - \underbrace{Q(x)\frac{dP}{dx}\tau\dot{x}(t)}_{Optical\ \ Damping}. \qquad \text{(S2.3)}$$

The first term on the right-hand side produces a nonlinear optical force, and the second term on the right-hand side provides optical damping, which is proportional to

the oscillator's velocity. Applying Eq. (S2.1) to Eq. (S2.3), the dynamic of the trapped sphere is described as

$$m\ddot{x} + m\left(\Gamma_g + Q(x)\frac{\tau}{m}\frac{dP}{dx}\right)\dot{x} + m\Omega_0^2 x - Q(x)P(x) = F_{th}, \tag{S2.4}$$

We calculate the optical force $Q(x)P(x)$ and optical damping rate $\gamma_{opt} = Q(x)\tau / m \cdot dP / dx$ by using the physical model given in ref. [S7] and the computational toolbox in ref. [S11]. Figure S2.1b shows an example of changes in these two terms when the oscillator moves along *x*-axis. We observe a strong nonlinear curve when the sphere leaves the original point (x = 0). This is in distinct contrast with the conventional optical tweezers where the optical force is approximately linear to the sphere's position. The inset in Fig. S2.2b illustrates an example of optical damping rate γ_{opt} as a function of sphere's displacement. The nonlinear response of the optical damping to oscillator's motion is clearly seen. Once the 3D translation stage is fixed, the optical damping rate γ_{opt} is reduced linearly with the oscillator's motion. Thus, optical damping term γ_{opt} can be fitted using a linear equation $\gamma_{opt} = \gamma_c x - \gamma_a$, as the red curve in the inset map. Then, the optical damping force in Eq. (S2.4) can be written as: $F_{damp} = m\gamma_c x\dot{x} - m\gamma_a \dot{x}$. The first term on the right-hand side implies a nonlinear modulation signal $\propto x\dot{x}$ which cools the sphere's motion. Similarly, the second term on the right-hand side implies a linear modulation signal $\propto -\dot{x}$ which amplifies the motion of the trapped sphere. The horizontal ordinate (Position x) can be regarded as the distance between the dual-beam optical tweezer and the active cavity in the experiment. By adjusting the 3D translation stage, appropriate parameters can be selected to realize phonon lasing.

2.2. PHONON DISTRIBUTION

When the oscillator experiences thermal dynamic, the phonon probability distribution can be described by a Boltzmann distribution,

$$p(n) = \sqrt{\left(\frac{m}{2\pi k_B T}\right)^3}\, 4\pi n^2 \exp\left[-\frac{mn^2}{2k_B T}\right], \tag{S2.7}$$

where m is the mass of the oscillator, k_B is Boltzmann constant, and T is the temperature.

For the case of coherent dynamic, the phonon probability distribution obeys Gaussian

distribution truncated at $n = 0$,

$$p(n) = \frac{1}{\sqrt{\pi n_{\max}}} \exp\left[-\frac{\left(n - n_0\right)^2}{n_{\max}} \right], \tag{S2.8}$$

where n_0 is mean phonon population $n_{max} = 2n_0 Q_M$, where $Q_M = n_0(g^{(2)}(0) - 1)$.

Reference

[S1] Zhang, J. et al. A phonon laser operating at an exceptional point. Nat. Photon. **12**, 479-484 (2018).

[S2] Kemiktarak, U., Durand, M., Metcalfe, M. & Lawall, J. Mode competition and anomalous cooling in a multimode phonon laser. *Phys. Rev. Lett.* **113**, 030802 (2014).

[S3] Pettit, R. M. et al. An optical tweezer phonon laser. *Nat. Photon.* **13**, 402-405 (2019).

[S4] Gieseler J., Deutsch B., Quidant R., & Novotny L., Subkelvin Parametric Feedback Cooling of a Laser-Trapped Nanoparticle. *Phys. Rev. Lett.* **109**, 103603 (2012).

[S5] Kiesel N., et al. Cavity cooling of an optically levitated submicron particle. *PNAS* 110(35), (2013).

[S6] Chang D. E., et al., Cavity opto-mechanics using an optically levitated nanosphere. *PNAS* 107(3) 1005-1010 (2010).

[S7] Kuang, T., et al. Optical confinement efficiency in the single beam intracavity optical tweezers. *Opt. Express* **28**, 35734-35747 (2020).

[S8] Zheng Y. et al., Robust optical-levitation-based metrology of nanoparticle's position and mass. *Phys. Rev.* Lett. **1249**, 223603 (2012).

[S9] Li T., Fundamental Tests of Physics with Optically Trapped Microspheres. *Springer* (2013).

[S10] Beresnev, S. A., Chernyak, V. G., & Fomyagin, G. A. Motion of a spherical particle in a rarefied gas. *J. Fluid Mech.* **219**, 405–421 (1990).

[S11] Callegari, A., Mijalkov, M., Gököz, A. B., & Volpe, G. Computational toolbox for optical tweezers in geometrical optics. *J. Opt. Soc. Am. B* **32**, B11–B19 (2015).